Letter

Amplification of electron-mediated spin currents by stimulated spin pumping

Benjamin Assouline, Marina Brik, Nirel Bernstein, and Amir Capua*
Department of Applied Physics, The Hebrew University of Jerusalem, Jerusalem 91904, Israel

(Received 7 October 2021; revised 15 September 2022; accepted 23 September 2022; published 25 October 2022)

Amplification of spin currents is attractive for fundamental research and practical applications. It has been recently discussed in the context of magnonic spin currents. However, amplification of spin currents that are mediated by electron transport is less familiar. Here we propose a stimulated spin pumping mechanism for amplifying ac electronic spin currents in a solid-state magnetic medium. The mechanism closely resembles the optical stimulated emission process during which a coherent photon is created. Two schemes are discussed: The first is synchronous and consists of phase-locked pulses that perturb a precessing magnetic moment. The second is asynchronous, where a precessing magnetic moment is driven by the dc spin Hall effect and inherently locks its phase during the interaction. Depending on the pulses' timing/dc bias level, the pumped spin current amplifies or absorbs the injected ac spin current mimicking the operation of the optical gain medium as seen from the gain saturation characteristics.

DOI: 10.1103/PhysRevResearch.4.L042014

Spin current amplifiers are necessary building blocks in spintronic networks. The advances in magnon spintronics as well as the expected advantages in efficient data processing, speed, and integration [1] have attracted much recent attention, and a variety of technologies for amplifying magnonic spin currents have emerged. Parallel pumping [2,3] was identified as a key mechanism offering superior performance for its magnon selectivity, while the spin Hall effect (SHE) approach was utilized to extend the magnon relaxation rate [4,5]. Even the topological magnon insulator [6] in which spin currents are carried by edge magnons was found suitable for amplification. Despite their necessity, amplifiers of spin currents that are mediated by electron transport have received little attention. Here we propose a process of stimulated spin pumping that we show to be capable of amplifying electron-mediated spin currents. The process closely resembles the optical stimulated emission during which a coherent photon is emitted.

Stimulated emission is a nonadiabatic (NA) process [7]. Namely, it is a hybrid time–frequency process whereby energy is transferred between an atomic system and a driving electromagnetic (EM) radiation before the two equilibrate. Traditionally, magnetic systems have been explored either in the time or frequency domains. The frequency domain ferromagnetic resonance (FMR) experiments [8–14] probes an adiabatic process since the EM field drives the magnetic system in a steady state, where energetic equilibrium pertains. Likewise, time domain free induction decay experiments [15–21] are also not NA because the driving EM field is absent.

Recently, the NA regime was demonstrated in ferromagnets (FMs) by combining the rf-driven FMR and the time-resolved magneto-optical Kerr effect [22]. In these experiments, the rf-driven magnetization precessions were perturbed by an optical pulse while the response was examined before the steady state was reached. Consequently, a variety of phenomena that are more familiar in their optical form were observed, including a controllable frequency chirping of the magnetization, induction of coherence in the inhomogeneously broadened spin ensemble, tuning of the intrinsic relaxation times, and mode locking of the spin ensemble [22,23]. The experiments were complemented by a rigorous theory of the NA regime in FM systems that are driven by EM radiation and spin currents [23].

The stimulated spin pumping amplification process described here takes the NA regime in FMs a step further. Two mechanisms are proposed, the first of which is synchronous and utilizes optical pulses that are phase locked with the injected electronic ac spin current and excite the NA regime in a FM. By tuning the amplitude and timing of the optical pulses, the injected ac spin current is either amplified or absorbed. The second mechanism relies on exciting first the spin transfer torque (STT) oscillator by a dc SHE. It is asynchronous since it does not require prior preparation of the phase of the excitation. Consequently, the injected ac spin current is amplified or absorbed, depending solely on the dc bias current level. We show that the operation of the asynchronous spin current amplifier is reminiscent of the operation of the optical amplifier, such as the erbium-doped fiber amplifier (EDFA) or the semiconductor optical amplifier (SOA), and that the similarity to the optical amplifier extends to the gain saturation profiles.

At the core of the spin current amplifier is a bilayer of a normal metal (NM)-FM as presented in Fig. 1(a). An ac charge current of amplitude $J_{C\,\mathrm{ac}}$ is passed through the NM

*amir.capua@mail.huji.ac.il

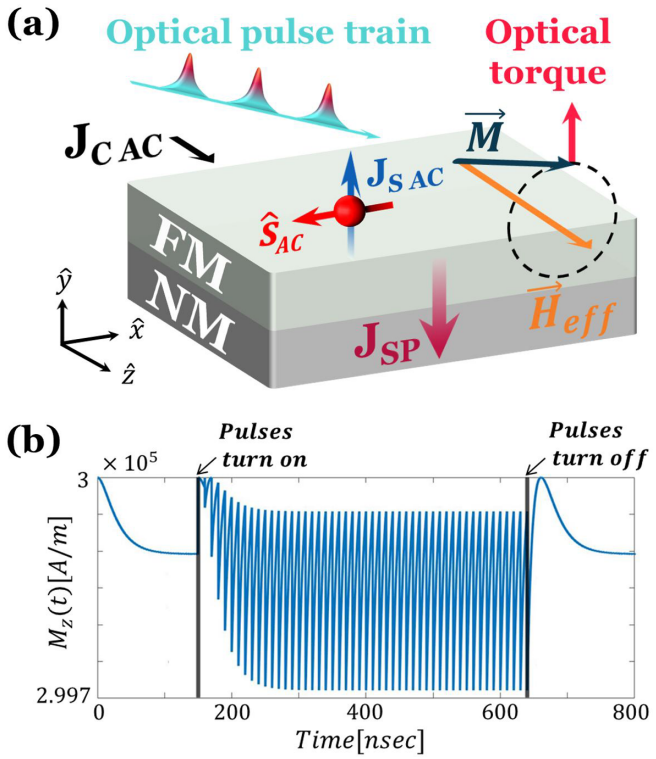

FIG. 1. Synchronous amplifier. (a) NM-FM bilayer configuration of the synchronous amplifier (b) $M_z(t)$ for amplification conditions. The optically induced magnetic field pulses were 0.05 T.

and generates an ac spin current of amplitude $J_{S\,\mathrm{ac}}$ by the SHE. The ac spin current is polarized in the $\hat{x}$ direction and drives the FMR in the presence of an effective magnetic field, $\vec{H}_{\mathrm{eff}}$. The anisotropy fields are neglected so that $\vec{H}_{\mathrm{eff}}$ is equal to the external magnetic field that is applied in the $\hat{z}$ direction and defines the energy axis. The magnitude of the external magnetic field is H_0 and is set to resonance. At the NM-FM interface, spin pumping takes place. So far, this process is identical to the STT-driven FMR [13]. Coherent spin current amplification takes place when the NA interaction is excited such that the pumped spin current, $\vec{J}_{SP}$, adds constructively to $\vec{J}_{S\,\mathrm{ac}}$ (vectors indicate spin orientation). An example of how the amplifier can be integrated in a spintronic circuit is illustrated in Supplemental Material Note S2 [24].

We start by addressing the synchronous amplification scheme. In this scheme, the NA regime in the FM is excited by applying a train of ultrashort optical pulses that momentarily demagnetize the FM and perturb the steady precessional state [15,17,22], as illustrated in Fig. 1(a). Also, other all-electrical means for achieving similar perturbations are possible. The pulses are phased locked with $\vec{J}_{S\,\mathrm{ac}}$ while each pulse is modeled as an effective instantaneous torque in the $\hat{y}$ direction. Using the Landau–Lifshitz–Gilbert–Slonczewski (LLGS) formalism under the macrospin approximation, we simulated 100-fs pulses at a repetition rate, Γ_{rep}, of 100 MHz, which represents realistic experimental conditions [25]. The temporal evolution of the $\hat{z}$ component of $\vec{M}$, M_z, is depicted in Fig. 1(b) for amplification conditions. Figure 1(b) shows the case where the relative phase, ϕ_{rf}, between the optical pulses and $\vec{J}_{S\,\mathrm{ac}}$ is such that $\vec{J}_{SP}$ is in phase with $\vec{J}_{S\,\mathrm{ac}}$, and amplification is maximal. We denote this condition by $\phi_{\mathrm{rf}} = 0^\circ$. Before turning on $J_{C\,\mathrm{ac}}$, $\vec{M}$ is aligned with $\vec{H}_{\mathrm{eff}}$. Once $J_{C\,\mathrm{ac}}$ is turned on, the generated $\vec{J}_{S\,\mathrm{ac}}$ drives the steady precessional state by STT. At $t = 150$ ns, the optical pulses are applied and initiate the spin mode locking [22] that excites the NA interaction. Over time, the steady NA interaction builds up and stabilizes at ~230 ns. In between pulses, M_z rises and the Zeeman energy decreases. This energy is transferred to $\vec{J}_{S\,\mathrm{ac}}$ by the emission of the spin pumping current, $\vec{J}_{SP}$. Depending on the relative phase between $\vec{J}_{SP}$ and $\vec{J}_{S\,\mathrm{ac}}$, which is denoted by $\phi_{J_{SP}-J_{S\,\mathrm{ac}}}$, $\vec{J}_{S\,\mathrm{ac}}$ is either amplified or absorbed.

The spin pumping is given by $\vec{J}_{SP} = \frac{\hbar}{4\pi M_s^2}\Re(g_{SP}^{\uparrow\downarrow})\vec{M} \times \frac{d\vec{M}}{dt}$ [26], where M_s is the magnetization saturation, $g_{SP}^{\uparrow\downarrow}$ is the spin pumping conductance at the NM-FM interface, and $\hbar$ is the reduced Planck constant. $\vec{J}_{SP}$ has the form of a damping-like torque and therefore increases the intrinsic Gilbert damping, α, by $\alpha_{SP} = \Re(g_{SP}^{\uparrow\downarrow})\frac{\gamma\hbar}{4\pi t_{\mathrm{FM}} M_s}$, where t_{FM} is the thickness of the FM layer.

The parameters of the simulation were chosen to model a Pt/CoFeB system [27] (listed in Supplemental Material Note S1 [24]), such that the relaxation time is long enough and the response builds up from pulse to pulse as shown in Fig. 1(b) for $t = 150$ to 230 ns. This condition is met when $\gamma\mu_0 H_0 \alpha < \Gamma_{\mathrm{rep}}$, where μ_0 is the permeability of the vacuum. On the other hand, when this condition is not fulfilled, each perturbation acts as an isolated event and the overall amplification drops significantly. The same principles described for amplification hold for absorption as well. This is achieved by setting $\phi_{\mathrm{rf}} = 180^\circ$, and is presented in Supplemental Material Fig. S2 [24]. In a broader context, the synchronous spin current amplification/absorption process is based on the same timing principles that dominate the Ramsey interferometry method of separated phase-shifted fields [28,29].

The gain characteristics of the synchronous amplifier are presented in Fig. 2. The amplified spin current $\vec{J}_{S\,\mathrm{out}}$ is a sum of $\vec{J}_{S\,\mathrm{ac}}$ and $\vec{J}_{SP}$. In our case, $\vec{J}_{S\,\mathrm{ac}}$ is polarized in the $\hat{x}$ direction. Accordingly, the spin current gain is given by $(\vec{J}_{S\,\mathrm{ac}} + \vec{J}_{SP})_x/(\vec{J}_{S\,\mathrm{ac}})_x$. Figure 2(a) illustrates the dependence of the gain on the relative timing of the pulses. It also presents the data for optically induced magnetic pulses of 0.01 to 0.05 T, in addition to a strong pulse of 0.15 T. For weak pulses (0.01 T and 0.02 T), the torque exerted by the pulses is insufficient to reach amplification independently of ϕ_{rf}, and the magnetization dynamics are primarily dictated by the STT induced by $\vec{J}_{S\,\mathrm{ac}}$. This is readily seen from the plots of $\phi_{J_{SP}-J_{S\,\mathrm{ac}}}$ of Fig. 2(b). For the 0.01-T and 0.02-T cases, $\phi_{J_{SP}-J_{S\,\mathrm{ac}}}$ is always between 90° and 180°, so that only destructive interference of $\vec{J}_{SP}$ and $\vec{J}_{S\,\mathrm{ac}}$ takes place.

As the pulses' magnitude increase, their influence becomes noticeable. By a process referred to as injection locking [30], $\vec{M}$ starts to follow the pulses and $\phi_{J_{SP}-J_{S\,\mathrm{ac}}}$ is set such that amplification can be reached as seen for 0.03 T and 0.05 T. As the intensity of the pulses is further increased, the STT arising from $\vec{J}_{S\,\mathrm{ac}}$ becomes negligible compared to the torque induced optically, and $\vec{M}$ is eventually locked solely to the pulses. This limit is illustrated in Fig. 2(b) for the case of strong 0.15-T pulses for which $\phi_{J_{SP}-J_{S\,\mathrm{ac}}}$ depends linearly on ϕ_{rf}. Generally, $\vec{J}_{SP}$ and $\vec{J}_{S\,\mathrm{ac}}$ add constructively when the pulses drive $\vec{M}$ such that the transverse (i.e., $\hat{x}$, $\hat{y}$) components of $\vec{M}$ and $\vec{J}_{SP}$ change

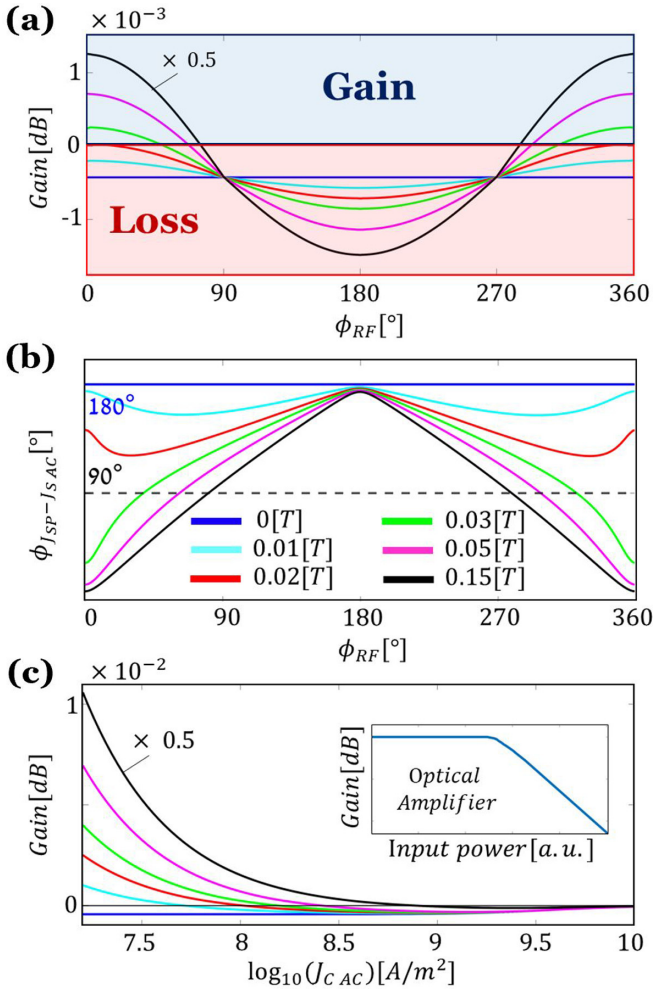

FIG. 2. Synchronous amplification. (a) $\phi_{\rm rf}$-dependent gain in dB ($\log_{10}[(\vec{J}_{S\ \rm ac}+\vec{J}_{SP})_x/(\vec{J}_{S\ \rm ac})_x]$). (b) $\phi_{\rm rf}$-dependent phase between the spin pumping and the injected ac spin current. (c) Gain saturation profiles for $\phi_{\rm rf}=0^\circ$. Inset presents the gain saturation of the optical amplifier. (a) and (b) are calculated for $J_{C\ \rm ac}=10^8$ A/m^2.

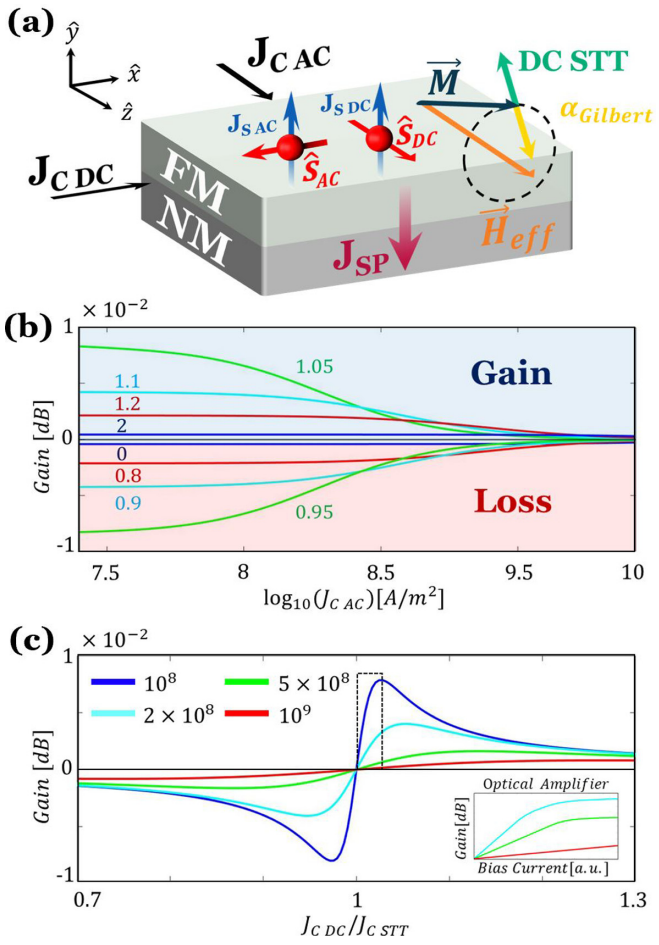

FIG. 3. Asynchronous spin current amplification. (a) Scheme of the STT oscillator used in the asynchronous amplification. (b) Gain saturation profiles for $J_{C\ \rm dc}$ of $0-2J_{C\ \rm STT}$. Symmetric $J_{C\ \rm dc}$ values with respect to $J_{C\ \rm STT}$ are plotted with the same color code. (c) Dependence of the gain on the dc spin current for $J_{C\ \rm ac}$ of 10^8-10^9 A/m^2. Inset presents qualitatively the bias current-dependent gain saturation profile of the optical amplifier for three levels of input optical power. The red solid line in the inset corresponds to the highest input power and magenta corresponds to the lowest.

sign compared to the unperturbed case. In the same manner, when the pulses are turned off at $t=640$ ns, M_z increases to its maximal value at $t=650$ ns, after which the phase of M_x is inverted and $\vec{J}_{SP}$ and $\vec{J}_{S\ \rm ac}$ add destructively again. A careful examination of M_x reveals a frequency chirping that is typical of a NA interaction [29] and has been addressed in FMs in Ref. [22] (see Supplemental Material Fig. S3 [24]).

The gain saturation profiles of the synchronous mechanism are presented in Fig. 2(c). The traces are plotted as a function $J_{C\ \rm ac}$. In contrast to the gain saturation profiles of the optical amplifier illustrated qualitatively in the inset, the spin current gain saturates monotonically already for very low $J_{C\ \rm ac}$ amplitudes. While in the optical amplifier such as the EDFA or SOA, the gain saturates due to carrier depletion at optical powers above the saturation power, the synchronous amplifier saturates already at weak inputs because the gain relies purely on the pulse's timing and magnitude. As $J_{C\ \rm ac}$ is increased, the ac STT overcomes the optically induced torque so that $\phi_{J_{SP}-J_{S\ \rm ac}}$ becomes closer to the initial destructive interference region and the gain eventually becomes negative. Since the system does not have any form of spin reservoir, saturation takes place immediately [31,32]. For extremely large $J_{C\ \rm ac}$, $\vec{J}_{SP}$ is eventually negligible compared to $\vec{J}_{S\ \rm ac}$ and the gain medium is transparent.

The second mechanism we discuss is asynchronous and is based on the STT-driven self-oscillations. In Fig. 3(a), $\vec{H}_{\rm eff}$ is set in the $\hat{z}$ direction and the oscillator is excited by injecting a dc charge current, $J_{C\ \rm dc}$, that is converted by the SHE to a dc spin current of magnitude $J_{S\ \rm dc}$ polarized in the $\vec{H}_{\rm eff}$ direction. Self-oscillations in the FM are obtained at the critical $J_{C\ \rm dc}$ value of $J_{C\ \rm STT}$, given by $J_{C\ \rm STT}=\frac{2eM_s t_{\rm FM}H_0}{\hbar\Theta_{\rm SHE}}\frac{\alpha+\alpha_{SP}}{1+(\alpha+\alpha_{SP})^2}$. Here as well, α_{SP} expresses the additional spin angular momentum losses that result from the spin pumping process. Amplification in this case is asynchronous. The phase of the STT oscillator is locked to $\vec{J}_{S\ \rm ac}$ and is determined during the first few cycles of the interaction. Depending on the magnitude of $J_{C\ \rm dc}$, $\vec{J}_{S\ \rm ac}$ is either amplified or absorbed. The gain saturation profiles are presented in Fig. 3(b). In contrast to the

synchronous amplifier, now the gain profiles resemble those of the optical amplifier: The small signal gain is constant and the gain saturates at large $J_{C\ \mathrm{ac}}$ values. The similarity to the optical amplifier stems from the analogy between the injection of incoherent carriers in the optical amplifier and the phase-less spins in the spin current amplifier. As a function of $J_{C\ \mathrm{dc}}$, the gain profiles are antisymmetric around the critical current so that when $J_{C\ \mathrm{dc}} < J_{C\ \mathrm{STT}}$, absorption takes place and, above $J_{C\ \mathrm{STT}}$, amplification is reached. This behavior is summarized in Fig. 3(c).

We explain the antisymmetry using the analogy to the Bloch vector formalism [33–35]. To this end, we transform $\vec{M}$ to the density matrix elements of a two-level system (TLS) according to $M_z = \rho_{11} - \rho_{22}$ and $\rho_{12} = (M_x - jM_y)/2$, where ρ_{11} and ρ_{22} are the occupation probabilities of the ground and excited states, respectively, and ρ_{12} is the off-diagonal term of the density matrix. Under this transformation, the LLGS equation describes the dynamics of an effective TLS as follows [32,36,37] (see Supplemental Material Note S3 [24]):

$$\begin{aligned}\dot{\rho}_{11} &= \Lambda_1 - \gamma_1\rho_{11} + 2[\Im(\rho_{12})\Re(V_{12}) - \Re(\rho_{12})\Im(V_{12})]\\ \dot{\rho}_{22} &= \Lambda_2 - \gamma_2\rho_{22} - 2[\Im(\rho_{12})\Re(V_{12}) - \Re(\rho_{12})\Im(V_{12})]\\ \dot{\rho}_{12} &= -(j\omega + \gamma_{\mathrm{inh}})\rho_{12} + j(\rho_{11} - \rho_{22})V_{12},\end{aligned} \tag{1}$$

where Λ_1 and Λ_2 are the injection rates into the ground and excited states, and γ_1 and γ_2 are the decay rates of the ground and excited states, respectively. ω is the natural resonance frequency of the TLS, γ_{inh} is the inhomogeneous broadening of the system, and V_{12} is the interaction term. γ_1 and γ_2 are related to α [23] and are introduced phenomenologically in the optical equations [36], in contrast to the Gilbert damping that describes a Rayleigh friction process [38]. Λ_1 and Λ_2 are relevant in the optical equations and are zero in our case. With the previous transformation, γ_1 and γ_2 are given by (see Supplemental Material Note S4 [24])

$$\begin{aligned}\gamma_1(M_z) &= -\gamma H_0 \frac{\alpha + \alpha_{SP}}{1 + (\alpha + \alpha_{SP})^2}\left(\frac{M_s - M_z}{M_s}\right)\left[1 - \frac{J_{C\ \mathrm{dc}}}{J_{C\ \mathrm{STT}}}\right]\\ \gamma_2(M_z) &= \gamma H_0 \frac{\alpha + \alpha_{SP}}{1 + (\alpha + \alpha_{SP})^2}\left(\frac{M_s + M_z}{M_s}\right)\left[1 - \frac{J_{C\ \mathrm{dc}}}{J_{C\ \mathrm{STT}}}\right].\end{aligned} \tag{2}$$

Since $M_z \leqslant M_s$, the term $\gamma H_0 \frac{\alpha+\alpha_{SP}}{1+(\alpha+\alpha_{SP})^2}(\frac{M_s \pm M_z}{M_s})$ is always non-negative, resulting in $\gamma_{1,2} \propto \mp[\,1 - \frac{J_{C\ \mathrm{dc}}}{J_{C\ \mathrm{STT}}}]$, so that above the critical current, γ_1 and γ_2 change signs. Amplification in the TLS occurs when the population is inverted—namely, when M_z is negative (see Supplemental Material Fig. S4 [24]). Below the critical current, $J_{C\ \mathrm{dc}} < J_{C\ \mathrm{STT}}$, $\gamma_2 > 0$, and $\gamma_1 < 0$, resulting in $M_z > 0$ and the population inversion is negative. Therefore, absorption takes place and $\phi_{J_{SP}-J_{S\ \mathrm{ac}}}$ is such that $\vec{J}_{SP}$ and $\vec{J}_S$ add destructively. Compared to the synchronous amplifier where $\phi_{J_{SP}-J_{S\ \mathrm{ac}}}$ is set by the optical pulses, here it is set by the population difference, $\rho_{11} - \rho_{22}$. Similarly, above the critical current, γ_1 and γ_2 change sign so that $\vec{M}$ amplifies $\vec{J}_{S\ \mathrm{ac}}$.

The transition from absorption to amplification around $J_{C\ \mathrm{STT}}$ is less abrupt the larger $J_{C\ \mathrm{ac}}$ is, as seen in Fig. 3(c). For small $J_{C\ \mathrm{ac}}$, the STT oscillator dictates the dynamics. In contrast, when $J_{C\ \mathrm{ac}}$ is large, e.g., for $J_{C\ \mathrm{ac}} = 10^9\ \mathrm{A/m^2}$, the ac STT dominates the dynamics and, in addition, the gain is saturated, as seen in Fig. 3(b). Therefore, the transition from absorption to amplification is moderate. At $J_{C\ \mathrm{dc}}$ values slightly beyond $J_{C\ \mathrm{STT}}$ of up to $\sim 1.04 \cdot J_{C\ \mathrm{STT}}$ [marked by the dashed black frame in Fig. 3(c)], the behavior resembles the bias current-dependent gain profile of the optical amplifier [39] presented in the inset of in Fig. 3(c). Beyond $\sim 1.04 \cdot J_{C\ \mathrm{STT}}$, the spin current gain decreases and the behavior of the spin and optical amplifiers deviate. We explain this deviation by the density matrix formalism. The amplified spin current is given by $(\vec{J}_{S\ \mathrm{out}})_x = (\vec{J}_{S\ \mathrm{ac}} + \vec{J}_{SP})_x$ in which $(\vec{J}_{SP})_x \propto M_y\dot{M}_z - \dot{M}_yM_z \approx \dot{M}_yM_z$ since M_z is slowly varying compared to M_y. This translates to $(\vec{J}_{SP})_x \propto (\dot{\rho}_{12} - \dot{\rho}_{21})(\rho_{11} - \rho_{22})$. At the critical current, transparency occurs—namely, $(\rho_{11} - \rho_{22}) = 0$. On the other hand, when $J_{C\ \mathrm{dc}} \gg J_{C\ \mathrm{STT}}$, $\vec{M}$ becomes antiparallel to $\vec{H}_{\mathrm{eff}}$ because of the large antidamping torque, and the transverse magnetization components decrease, resulting in $\dot{\rho}_{12},\ \dot{\rho}_{21} \to 0$. Therefore, $(\vec{J}_{SP})_x \to 0$ in both limits. It is also seen that the expression for $(\vec{J}_{SP})_x$ is antisymmetric with respect to the transparency point at $J_{C\ \mathrm{STT}}$.

Finally, we point out an additional difference between the spin current amplifier and the optical amplifier that is found in the dc excitation process. In the TLS optical amplifier model, the incoherent current injection increases ρ_{11}, ρ_{22} [32,40], as illustrated in Eq. (1) by the term $\Lambda_{1,2}$. In contrast, in the density matrix formalism of the spin current amplifier, the incoherent spin injection manifests through the decay terms, e.g., $\gamma_{1,2}$ in Eq. (2), by the antidamping STT according to the LLGS equation.

In summary, we present two mechanisms for amplifying electronic ac spin currents by stimulated spin pumping. The first mechanism is synchronous and provides control over the phase of the pumped spin current thereby revealing the inner workings of the NA amplification process. The second mechanism is asynchronous and is a closer analogue of the optical amplifier. The similarity stems from the dynamics of converting incoherent carriers/spins into coherent carriers/spins. Our findings stimulate further connections between well-established concepts from laser physics and spintronics technology. For example, a saturable spin current absorber that gives rise to a mode-locked spin current emission capable of exerting a torque that is stronger than observed to date may be considered. Likewise, Gilbert-type loss terms that benefit from a rigorous physical origin can be introduced into the optical TLS. Future work should relate to spatially distributed traveling wave propagation effects and, most importantly, to the experimental realization of the spin current amplifier.

A.C. and B.A. acknowledge the support from the Israel Science Foundation (Grant No. 1217/21), the Peter Brojde Center for Innovative Engineering and Computer Science, and from the Center for Nanoscience and Nanotechnology of the Hebrew University of Jerusalem.

[1] P. Pirro, V. I. Vasyuchka, A. A. Serga, and B. Hillebrands, Advances in coherent magnonics, Nat. Rev. Mater. **6**, 1114 (2021).

[2] T. Brächer, P. Pirro, and B. Hillebrands, Parallel pumping for magnon spintronics: Amplification and manipulation of magnon spin currents on the micron-scale, Phys. Rep. **699**, 1 (2017).

[3] A. Kamimaki, S. Iihama, K. Z. Suzuki, N. Yoshinaga, and S. Mizukami, Parametric Amplification of Magnons in Synthetic Antiferromagnets, Phys. Rev. Appl. **13**, 044036 (2020).

[4] O. Gladii, M. Collet, K. Garcia-Hernandez, C. Cheng, S. Xavier, P. Bortolotti, V. Cros, Y. Henry, J.- V. Kim, A. Anane, and M. Bailleul, Spin wave amplification using the spin Hall effect in permalloy/platinum bilayers, Appl. Phys. Lett. **108**, 202407 (2016).

[5] B. Divinskiy, V. E. Demidov, S. Urazhdin, R. Freeman, A. B. Rinkevich, and S. O. Demokritov, Excitation and amplification of spin waves by spin–orbit torque, Adv. Mater. **30**, 1802837 (2018).

[6] D. Malz, J. Knolle, and A. Nunnenkamp, Topological magnon amplification, Nat. Commun. **10**, 3937 (2019).

[7] I. I. Rabi, Space quantization in a gyrating magnetic field, Phys. Rev. **51**, 652 (1937).

[8] S. S. Kalarickal, P. Krivosik, M. Wu, C. E. Patton, M. L. Schneider, P. Kabos, T. J. Silva, and J. P. Nibarger, Ferromagnetic resonance linewidth in metallic thin films: Comparison of measurement methods, J. Appl. Phys. **99**, 093909 (2006).

[9] G. Woltersdorf and C. H. Back, Microwave Assisted Switching of Single Domain $Ni_{80}Fe_{20}$ Elements, Phys. Rev. Lett. **99**, 227207 (2007).

[10] J. M. Beaujour, D. Ravelosona, I. Tudosa, E. E. Fullerton, and A. D. Kent, Ferromagnetic resonance linewidth in ultrathin films with perpendicular magnetic anisotropy, Phys. Rev. B **80**, 180415(R) (2009).

[11] Y. Zhao, Q. Song, S.- H. Yang, T. Su, W. Yuan, S. Parkin, J. Shi, and W. Han, Experimental investigation of temperature-dependent Gilbert damping in permalloy thin films, Sci. Rep. **6**, 22890 (2016).

[12] S. O. Demokritov, V. E. Demidov, O. Dzyapko, G. A. Melkov, A. A. Serga, B. Hillebrands, and A. N. Slavin, Bose-Einstein condensation of quasi-equilibrium magnons at room temperature under pumping, Nature (London) **443**, 430 (2006).

[13] L. Liu, T. Moriyama, D. C. Ralph, and R. A. Buhrman, Spin-Torque Ferromagnetic Resonance Induced by the Spin Hall Effect, Phys. Rev. Lett. **106**, 036601 (2011).

[14] Y. Wang, R. Ramaswamy, and H. Yang, FMR-related phenomena in spintronic devices, J. Phys. D Appl. Phys. **51**, 273002 (2018).

[15] E. Beaurepaire, J. C. Merle, A. Daunois, and J. Y. Bigot, Ultrafast Spin Dynamics in Ferromagnetic Nickel, Phys. Rev. Lett. **76**, 4250 (1996).

[16] T. J. Silva, C. S. Lee, T. M. Crawford, and C. T. Rogers, Inductive measurement of ultrafast magnetization dynamics in thin-film permalloy, J. Appl. Phys. **85**, 7849 (1999).

[17] B. Koopmans, M. van Kampen, J. T. Kohlhepp, and W. J. M. de Jonge, Ultrafast Magneto-Optics in Nickel: Magnetism Or Optics? Phys. Rev. Lett. **85**, 844 (2000).

[18] M. van Kampen, C. Jozsa, J. T. Kohlhepp, P. LeClair, L. Lagae, W. J. M. de Jonge, and B. Koopmans, All-Optical Probe of Coherent Spin Waves, Phys. Rev. Lett. **88**, 227201 (2002).

[19] J.- Y. Bigot, M. Vomir, and E. Beaurepaire, Coherent ultrafast magnetism induced by femtosecond laser pulses, Nat. Phys. **5**, 515 (2009).

[20] I. Radu, G. Woltersdorf, M. Kiessling, A. Melnikov, U. Bovensiepen, J. U. Thiele, and C. H. Back, Laser-Induced Magnetization Dynamics of Lanthanide-Doped Permalloy Thin Films, Phys. Rev. Lett. **102**, 117201 (2009).

[21] T. M. Spicer, C. J. Durrant, P. S. Keatley, V. V. Kruglyak, W. Chen, G. Xiao, and R. J. Hicken, Current-induced picosecond magnetization dynamics in a Ta/CoFeB/MgO Hall bar, J. Phys. D Appl. Phys. **52**, 355003 (2019).

[22] A. Capua, C. Rettner, S.- H. Yang, T. Phung, and S. S. P. Parkin, Ensemble-averaged Rabi oscillations in a ferromagnetic CoFeB film, Nat. Commun. **8**, 16004 (2017).

[23] M. Brik, N. Bernstein, and A. Capua, Coherent control in ferromagnets driven by microwave radiation and spin polarized current, Phys. Rev. B **102**, 224308 (2020).

[24] See Supplemental Material at http://link.aps.org/supplemental/10.1103/PhysRevResearch.4.L042014 for simulation parameters, practical application scheme, Bloch vector formalism, and TLS decay rates calculation.

[25] N. Bernstein, M. Brik, B. Assouline, S.- H. Yang, and A. Capua (unpublished)).

[26] K. Sato and E. Saitoh, *Spintronics for Next Generation Innovative Devices* (Wiley, Chichester, 2015).

[27] A. Capua, T. Wang, S.- H. Yang, C. Rettner, T. Phung, and S. S. P. Parkin, Phase-resolved detection of the spin Hall angle by optical ferromagnetic resonance in perpendicularly magnetized thin films, Phys. Rev. B **95**, 064401 (2017).

[28] M. O. Scully and M. S. Zubairy, *Quantum Optics* (Cambridge University Press, Cambridge, 1997).

[29] A. Capua, O. Karni, G. Eisenstein, V. Sichkovskyi, V. Ivanov, and J. P. Reithmaier, Coherent control in a semiconductor optical amplifier operating at room temperature, Nat. Commun. **5**, 5025 (2014).

[30] C. L. Tang and H. Statz, Phase-locking of laser oscillators by injected signal, J. Appl. Phys. **38**, 323 (1967).

[31] A. Capua, O. Karni, G. Eisenstein, and J. P. Reithmaier, Rabi oscillations in a room-temperature quantum dash semiconductor optical amplifier, Phys. Rev. B **90**, 045305 (2014).

[32] A. Capua, O. Karni, and G. Eisenstein, A finite-difference time-domain model for quantum-dot lasers and amplifiers in the Maxwell & Schrodinger framework, IEEE J. Sel. Top. Quantum Electron. **19**, 1900410 (2013).

[33] R. P. Feynman, F. L. Vernon, and R. W. Hellwarth, Geometrical representation of the Schrödinger equation for solving maser problems, J. Appl. Phys. **28**, 49 (1957).

[34] G. Klughertz, L. Friedland, P.- A. Hervieux, and G. Manfredi, Autoresonant switching of the magnetization in single-domain nanoparticles: Two-level theory, Phys. Rev. B **91**, 104433 (2015).

[35] G. Klughertz, L. Friedland, P.- A. Hervieux, and G. Manfredi, Spin-torque switching and control using chirped AC currents, J. Phys. D Appl. Phys. **50**, 415002 (2017).

[36] M. Sargent, M. Scully, and W. Lamb, *Laser Physics* (CRC Press, Boca Raton, FL, 1974).

[37] L. Allen and J. Eberly, *Optical Resonance and Two Level Atoms* (Dover Publications, New York, 1987).

[38] T. L. Gilbert, A phenomenological theory of damping in ferromagnetic materials, IEEE Trans. Magnet. **40**, 3443 (2004).

[39] P. Berger, M. Alouini, J. Bourderionnet, F. Bretenaker, and D. Dolfi, Dynamic saturation in semiconductor optical amplifiers: Accurate model, role of carrier density, and slow light, Opt. Express **18**, 685 (2010).

[40] J. Yao, G. P. Agrawal, P. Gallion, and C. M. Bowden, Semiconductor laser dynamics beyond the rate-equation approximation, Optics Commun. **119**, 246 (1995).